Journal of Magnetism and Magnetic Materials 472 (2019) 66–73

Contents lists available at ScienceDirect

Journal of Magnetism and Magnetic Materials

journal homepage: www.elsevier.com/locate/jmmm

Research articles

Effect of magnetic nanoparticles coating on cell proliferation and uptake

Vlasta Zavisova[a,*], Martina Koneracka[a], Alena Gabelova[b], Barbora Svitkova[b], Monika Ursinyova[c], Martina Kubovcikova[a], Iryna Antal[a], Iryna Khmara[a,e], Alena Jurikova[a], Matus Molcan[a], Miloš Ognjanović[d], Bratislav Antić[d], Peter Kopcansky[a]

[a] Institute of Experimental Physics, Slovak Academy of Sciences, Watsonova 47, Kosice, Slovakia
[b] Biomedical Research Center SAS, Slovak Academy of Sciences, Dubravska cesta 9, Bratislava, Slovakia
[c] Slovak Medical University, Limbova 12, Bratislava, Slovakia
[d] The Vinca Institute of Nuclear Sciences, University of Belgrade, M. Petrovića Alasa 12–14, Belgrade, Serbia
[e] Pavol Jozef Safarik University, Faculty of Science, Park Angelinum, Kosice, Slovakia

ARTICLE INFO

Keywords:
Magnetic nanoparticles
Magnetic fluid
Magnetic hyperthermia
Cytotoxicity
Cell uptake

ABSTRACT

Magnetic iron oxide nanoparticles (MNPs) are one of the most promising types of nanoparticles for biomedical applications, primarily in the context of nanomedicine-based diagnostics and therapy. They are used as contrast agents in magnetic resonance imaging and magnetite cell labelling. Furthermore, they are promising heating mediator in magnetic hyperthermia-based therapy, and can serve as nanocarriers in targeted gene and drug delivery as well. In biomedical applications, coating plays an important role in nanoparticle dispersion stability and biocompatibility. However, the impact of nanoparticle surface chemistry on cell uptake and proliferation has not been sufficiently investigated. The objective of this study is to prepare magnetic nanoparticles with inner magnetite core and hydrophilic outer shell of surfactant, protein and polymers that are commonly used in biomedical research. MNPs were characterized in-depth by various physicochemical methods. Magnetic hyperthermia, applied to find out the influence of MNPs coating on heating characteristics of the samples, did not show any correlation between layer thickness and specific adsorption rate. To evaluate the impact of surface chemistry on cell proliferation and internalization, the human lung adenocarcinoma epithelial (A549) cells were utilized. Substantial differences were determined in the amount of internalized MNPs and cell viability in dependence on surface coating. Our results indicate that the surface chemistry not only protects particles from agglomeration but also affect the interaction between cell and MNPs.

1. Introduction

The application of nanotechnology to medicine provides an opportunity to study the biological systems at a subtler level, giving rise to better understanding of disease mechanisms. Moreover, nanomaterials enable more accurate and rapid diagnosis, targeted and effective drug delivery, and novel ways of organ and tissue regeneration. The biocompatibility and colloidal stability of nanoparticles (NPs) in physiological solutions is imperative for their development for clinical use [1]. Surface modification of particles with surfactants or polymers protects particles from aggregation and agglomeration, prolongs the blood circulation time and facilitates their further functionalization (*i.e.* binding of specific ligands, antigen, aptamer, protein etc. on the surface of NPs) to increase their accumulation in a tumour region [2]. Several methods and numerous coating agents have been developed and employed for modifying the surface properties of the magnetite nanoparticles (MNPs) [3–6]. One of the suitable compounds to improve colloidal stability of MNPs is polyethylene glycol (PEG), a non-degradable polyether of the monomer ethylene glycol. Water-solubility, low toxicity together with outstanding biocompatibility and bio-inertness, make PEG the most frequently used coating polymer among biomaterials. Highly hydrated PEG chains exhibit steric repulsion based on an osmotic or entropic mechanism [7]. Bovine serum albumin (BSA) has been used as a versatile protein carrier for drug delivery as well as coating protein. BSA possesses non-toxic, non-immunogenic, biocompatible and biodegradable properties [3,4]. Polymer nanoparticles created by poly(D,L-lactide-*co*-glycolide) (PLGA) and polylactic acid (PLA) are FDA-approved biodegradable and biocompatible nanomaterials, especially for cancer-related human applications [8,9]. Their main advantage is that they easily undergo degradation due to the hydrolysis of the ester bond, and the hydrolysis products are metabolized and removed from the body *via* normal metabolic pathways [6]. These nanocarriers are stable in the

* Corresponding author.
E-mail address: zavisova@saske.sk (V. Zavisova).

https://doi.org/10.1016/j.jmmm.2018.09.116
Received 25 June 2018; Received in revised form 17 September 2018; Accepted 28 September 2018
Available online 03 October 2018
0304-8853/

blood, are non-toxic, non-immunogenic, non-inflammatory, and do not promote thrombosis or affect the reticuloendothelial system [5].

The effect of surface chemistry on cell-nanoparticle interaction remains unclear despite intensive research in this field. To better understand the impact of coating on MNP uptake and cell viability, we synthesized MNPs with different surface modification, in particular with PEG, BSA and PLGA. MNPs were characterized in-depth by various physicochemical methods, and their biocompatibility was investigated in human lung cells A549. We analysed the capacity of surface modified MNPs to internalize into cells, and their effect on cell morphology and viability.

2. Materials and methods

2.1. Material

Ferric chloride hexahydrate ($FeCl_3{\cdot}6H_2O$), ferrous sulphate heptahydrate ($FeSO_4{\cdot}7H_2O$), ammonium hydroxide (NH_4OH), sodium oleate ($C_{17}H_{33}COONa$), poly(ethylene glycol) with average molecular weight (M_W) 1 kDa, PLGA with a D,L-lactide to glycolide ratio 85:15, M_W 50–75 kDa, bovine serum albumin and pluronic F68, were provided by Sigma Aldrich. All compounds were used without any further treatment.

2.2. Cell culture

The human lung adenocarcinoma epithelial cell line A549 were maintained in Dulbecco's modified Eagle medium (DMEM) supplemented with 10% fetal bovine serum (FBS) and antibiotics (penicillin, 100 U/mL; streptomycin and kanamycin, 100 μg/mL). The cell lines were cultured in a humidified atmosphere of 5% CO_2 at 37 °C. In all experiments, cells were exposed to nanoparticles in medium supplemented with 2% FBS.

2.3. Synthesis of magnetic nanoparticles and surface coating

The magnetic iron oxide (Fe_3O_4) nanoparticles were synthesized by chemical co-precipitation of ferric and ferrous salts in alkaline aqueous medium [6,10]. Firstly, $FeSO_4{\cdot}7H_2O$ and $FeCl_3{\cdot}6H_2O$ in molar proportion of 1:2 were dissolved in deionized water, and then NH_4OH solution was added into the solution under constant stirring. The black precipitate was mixed thoroughly and subsequently washed several times with water by magnetic decantation. The colloidal suspension of MNPs was stabilized by the formation of a bilayer of the sodium oleate surfactant. Sodium oleate (SO, 70 wt% with respect to Fe_3O_4) was added to the nanoparticle suspension and mixed under heating until the boiling point was reached [11,12]. This stable colloidal suspension of the MNPs dispersed in water is referred hereafter as magnetic fluid (MF).

2.4. Modification of nanoparticles

MF nanoparticles were further coated with the polymer, poly (ethylene glycol) (PEG) according to the process described by Závišová et al. [13–15]. PEG prolongs the circulation time of nanoparticles. The mixture of PEG water solution and MF suspension was incubated in a horizontal shaker for 24 h at 40 °C and 200 rpm. The PEG/magnetite weight ratio was equal to 0.25. Further on, the resulting stable colloid sample consisting of MNP suspension modified by PEG is referred to as MFPEG.

To improve the biocompatibility of MF, bovine serum albumin (BSA) in weight ratio of $BSA/Fe_3O_4 = 2$ was used [12]. BSA strongly reduces the non-specific interactions with the plasma protein. The mixture was incubated in a horizontal shaker for 6 h at 40 °C and 200 rpm. Then, pH of the colloid was adjusted to value of 7.4 by phosphate buffer. The resulting sample consisting of MF modified by BSA is referred to as MFBSA.

2.5. Preparation of magnetic polymer nanospheres

A modified nanoprecipitation method [16] was used to prepare magnetic polymer nanospheres. Briefly, 100 mg of PLGA was dissolved in 10 mL acetone to prepare a polymer solution. Next, the aqueous solution was prepared by mixing 5 mL pluronic F68 (1.25 mg/mL in water) as a stabilizing agent and 2 mL of water-based MFPEG (60 mg Fe_3O_4/mL). The organic phase was added dropwise into the aqueous solution and stirred vigorously for several hours to allow for complete evaporation of the organic solvent at room temperature. A turbid nanoparticle suspension was formed (PLGA-MFPEG).

All prepared samples were washed by water by centrifugation at 18,000 rpm for 2 h to remove unbound compounds.

2.6. Particle size determination

2.6.1. Transmission electron microscopy

The particle size, size distribution and morphology were determined by transmission electron microscopy (TEM) with a Tesla BS 500 microscope normally operated at 90 kV with 80,000× magnification by the replication technique. Samples were prepared by placing a drop of the water diluted sample onto a carbon-coated copper grid and allowing it to dry at room temperature. The size distributions were determined by manual measurement of more than 100 particles using the software ImageJ.

2.6.2. Scanning electron microscopy

Scanning electron microscopy (SEM, JEOL7000F microscope) was used to evaluate the morphology and microstructure of the coated nanoparticles in the prepared samples. A droplet of the colloidal dispersion was first diluted in water and then deposited on the SEM sample stub and dried under vacuum prior to sputtering with carbon and subsequent observation.

2.6.3. Dynamic light scattering method (DLS)

DLS is a technique for measuring the size of particles typically in the nanometer region. DLS-method is based on measuring of fluctuations of intensity of scattered light by small volume of colloidal solution. Fluctuations of light intensity are related to the intensive Brownian motion of the colloidal particles. The velocity of the Brownian motion is defined by a translational diffusion coefficient. Depending on the shape of the MNP, for spherical particles, the hydrodynamic radius of the particle R_H was calculated from its diffusion coefficient by the Stokes-Einstein equation $D_f = k_BT/6\pi\eta R_H$, where k_B is the Boltzmann constant, T is the temperature of the suspension, and η is the viscosity of the surrounding medium.

For hydrodynamic particle size measurement of prepared samples, Zetasizer Nano ZS from Malvern Instruments (UK) equipped with a He–Ne laser (633 nm) and operating at scattering angle of 173 °C and a temperature of 20 °C was applied.

Particle size distribution and zeta potential of surface-modified MNPs in culture medium at 37 °C were determined by DLS using Zetasizer Nano-ZS (Malvern Instruments, UK) equipped with a 4 mW helium/neon laser ($\lambda = 633$ nm) and a thermoelectric temperature controller. The measurements were performed at ~3 min intervals during 24 h; every data point was recorded as the average of at least 11 repetitions. The characteristics of MNPs and culture medium have already been published elsewhere [17].

2.6.4. Magnetic measurements (Langevin fit)

It is possible to determine the particle-size distribution from magnetic measurements. If an ideal sample is measured in the superparamagnetic state, then the magnetization is simply given by the integration of the Langevin function Eq. (1) for each particle size in the distribution [18]. The field dependent magnetization measurements were performed using Magnetic Property Measuring System model

MPMS-XL-5 (Quantum Design) equipped with 5 T superconducting magnet.

In order to estimate the particle size and the width of the size distribution, the positive quadrant part of the curve was fitted to the classical Langevin function weight-averaged with the modified log-normal PSD of Eq. (1):

$$M = M_s \int_0^\infty L(\xi) f(x) dx \tag{1}$$

where M_S is the saturation magnetization, $L(\xi) = coth(\xi) - 1/\xi$, is the Langevin function with $\xi = \mu_0 \mu H/k_B T$, μ_0 is the magnetic permeability of vacuum, μ *is* magnetic moment, H is the magnetic field strength, k_B is the Boltzmann constant and T is the absolute temperature. The particle size distribution in this case is usually described by log-normal distribution:

$$f(x) = \frac{1}{xs\sqrt{2\pi}} exp\left[-\frac{ln^2\left(\frac{x}{D_0}\right)}{2s^2}\right] \tag{2}$$

where x is the magnetic diameter, D_0 and s are the parameters determined from the magnetization curve. We used the fitting procedure introduced by Rozynek [19]. On the basis of these parameters, the mean diameter $< d >$ and standard deviation of particle size σ can be determined from the formulae:

$$<d> = D_0 exp\left(\frac{s^2}{2}\right) \tag{3}$$

$$\sigma = D_0 exp\left(\frac{s^2}{2}\right)\sqrt{exps^2 - 1} \tag{4}$$

2.7. Zeta potential measurements

Zeta potential is a physical property exhibited by all particles in suspension that can be quantified using an electrophoretic mobility measurement. Zeta potential has long been recognized as a good index of the magnitude of the charge interaction between colloidal particles, and its measurement is commonly used to predict and control the stability of colloidal systems. If all the particles in suspension have a large negative or positive zeta potential, then they will tend to repel each other and there will be no tendency for the particles to come together. However, if the particles have low absolute value of zeta potential then there will be no force to prevent the particles coming together and flocculating. The dividing line between stable and unstable suspensions is generally taken at either +30 or −30 mV.

The zeta potential of all prepared samples was measured at 25 °C in the apparatus used for DLS.

2.8. Measurement of particle heat generation by alternating magnetic field (AMF) calorimetry

Calorimetric measurements for all studied samples (with magnetite concentration of 5 mg/mL) were performed by commercial AC applicator (model DM100 nanoScale Biomagnetic, Spain). Temperature evolution curves in time were recorded under an AMF with applied intensity H up to ~24 kA/m and frequency $f = 252$ kHz for 160 s. Temperature of the samples was monitored by fibre optical probe immersed in the 1 mL of NPs suspension.

2.9. Thermogravimetric analysis (TGA)

TGA was carried out to determine the amount of modifying compound adsorbed on the magnetic nanoparticles. For this purpose, the washed samples were freeze-dried in a lyophilizer at −52 °C. TG experiments were performed on the dried samples under flowing air in the temperature range of 20–700 °C with the heating rate of 10 °C/min using TGDTA Setaram SETSYS 16 apparatus.

2.10. Treatment of cells

Exponentially growing cells were exposed to different concentrations of MF, MFPEG, MFBSA and PLGA-MFPEG nanoparticles for 24 h. The viability of cells after exposure to MNPs differing in surface coating was evaluated in the concentration range 0–1.2 mM (0–277.80 μg/mL). The unit mM (mmol/L) of iron oxide was used to express the MNPs concentrations; under these conditions, equal numbers of particles were applied to human lung cells regardless of the surface coating. Concentrations of surface modified MNPs expressed in μg/mL as well as in μg/cm^2 are presented in Table S1. The treatment of the cells was finished by removing the medium and washing the cells twice with phosphate buffer saline (PBS). Then the cells were processed immediately.

2.11. Atomic absorption spectrometry (AAS)

AAS was adapted to quantify the cellular uptake of MNPs. Duplicate analyses were carried out by flame atomic absorption spectrometry for Fe. The digestion of cell pellet was realized with 500 μL of 65% HNO_3 (Suprapure) in ultrasonic bath at 85 °C for 5 h. The digests were then diluted with 2% HNO_3 in deionized water. The instrumental parameters for Fe determination were: wavelength 248.3 nm, slit width: 0.2 nm, flame type: acetylene-air, flow: 2.0 L/min for acetylene and 13.5 L/min for air, deuterium background correction, method of calibration curve in the range 0.1–10 mg/L. The limit of detection (LOD) and limit of quantification (LOQ) for the present method were 0.007 mg/L and 0.025 mg/L, respectively.

2.12. Time-lapse imaging of cells

Exponentially growing A549 cells seeded in 24-well plates were treated with surface modified MNPs. Phase-contrast images were taken in the IncuCyte ZOOMTM Live Content Imaging System (Essen BioScience, Hertfordshire, UK) at 2 h intervals. Cell morphology and confluence were screened using IncuCyte ZOOM 2013A software as recommended by the manufacturer.

2.13. Cytotoxicity of surface coated MNPs

The 3-(4,5-dimethyl thiazol-2-yl)-2,5-diphenyl tetrazolium bromide (MTT) assay based on the protocol described by Mosmann [20] was used with minor modifications. Briefly, viability of A549 was carried out in plastic 96-well cell culture cluster plates at 4×10^3 cells/well and photometric evaluation (at 540 nm excitation and 690 nm emission wavelengths) using the Multiskan Multisoft plate reader (Labsystems, Finland) and Genesis software provided by the producer. IC_{50} values were calculated from the dose–response curves using CalcuSyn software (Biosoft, Cambridge, UK). Since the colour of magnetic nanoparticles interferes with the spectrophotometry readings when up by the cells, the net readings were corrected with a net particle reading according to Hafeli et al. [21].

3. Results and discussion

3.1. Physical-chemical characterization of MNPs

The X-ray diffraction measurement confirmed the magnetite inner core with a mean diameter 6.6 ± 0.1 nm in MF [22]. TEM images of unmodified MF and modified MF samples are shown in Fig. 1AB (I) and AB (II-IV), respectively. While TEM microscopic evaluation allow us to "really" see the particles and evaluate their range of shapes and sizes, SEM microscope visualize surface morphology, dispersed and

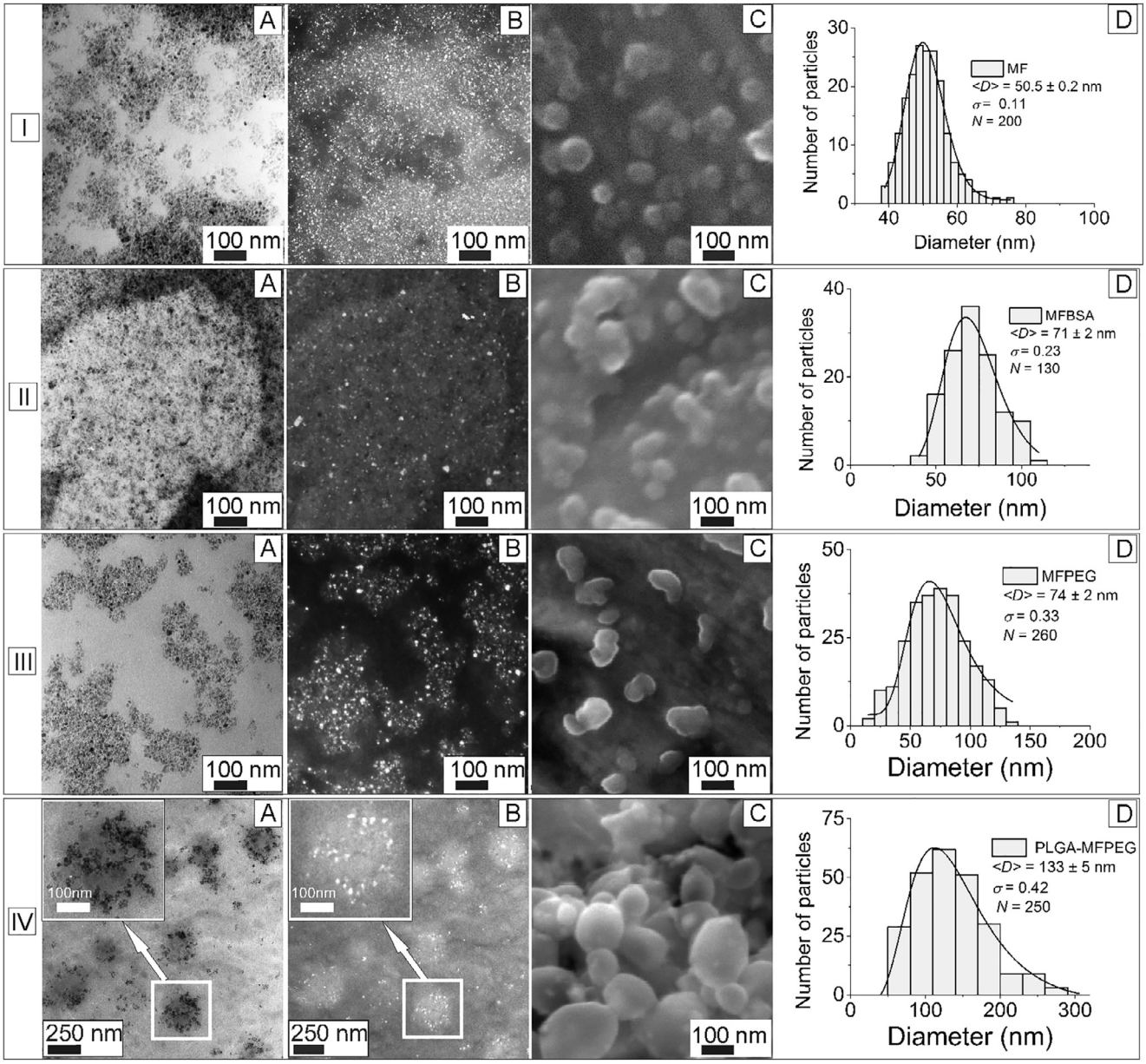

Fig. 1. TEM image of MNPs in MF (I), MFBSA (II), MFPEG (III), PLGA-MFPEG (IV) in a bright field mode (A) and in dark field (B), SEM images of MNPs (C), and corresponding particle size distributions determined from SEM images (D).

Table 1
Basic physicochemical characteristics of MNPs in MF, MFBSA, MFPEG, and PLGA-MFPEG. The magnetic core diameter obtained from Langevin fit (D_{LF}), the MNPs diameters obtained from SEM images (D_{SEM}) and DLS characterization (D_{DLS}), polydispersity index (PDI), zeta potential, saturation magnetization (*Ms*), weight loss and weight ratio of modifying compounds (SO, BSA, PEG, PLGA)/Fe_3O_4, and SAR values.

Sample	D_{LF} (nm)	D_{SEM} (nm)	D_{DLS} (nm)	*PDI*	Zeta potential (mV)	*Ms* (emu/g)	Modifying compound weight loss (wt%)	Modifying compound/Fe_3O_4 (mg/mg)	*SAR* (W/g) (252 kHz, 23.9 kA/m)
MF	10.6	50.5 ± 0.2	44	0.10	−42	2.66	26	0.35	13.4
MFBSA	10.1	71 ± 2	70	0.16	−37	2.74	11	0.23	14.6
MFPEG	10.0	74 ± 2	76	0.12	−42	2.06	4	0.08	13.6
PLGA-MFPEG	10.0	133 ± 5	155	0.13	−50	1.87	35	1.02	15.9

agglomerated nanoparticles, and surface functionalizations. SEM is considered to be an absolute measurement of particle size (including magnetic core and coating layer). SEM images (Fig. 1C (I-IV)) analyses determined irregularly-shaped quasi-spherical MNPs with primarily smooth surface. The number of nanoparticles subjected to analysis, the average particle diameter, and the corresponding standard deviation are summarized in each corresponding histogram. The particle size of unmodified MF was measured as 50.5 ± 0.2 nm (Fig. 1D (I)). The particle size of BSA modified MF (Fig. 1D (II)) was determined as 71 ± 2 nm. The particle sizes of MFPEG (Fig. 1D (III)) and PLGA-MFPEG (Fig. 1D (IV)) were 74 ± 2 nm and 133 ± 5 nm, respectively. Size data from the analysis were divided into bins, and Origin 8

software was used for lognormal fits. As a result, average size (D_{SEM}) and geometric standard deviation (σ) are reported in histograms. Number of measured particles was sufficient (over 100) in all studied samples and are included in the relevant histograms. The size of nanoparticles increased proportionally with the surface coating. The mean diameters obtained by fitting histograms by log-normal distribution function are summarized in Table 1. DLS was also used to characterize the prepared sample solutions from which the samples for microscopy were made. This technique differs in many aspects from imaging of dried samples, and is sensitive to dynamic aggregation, aggregation, agglomeration, etc. Thus, there are several reasons to expect different results from this technique compared to the microscopic techniques. In spite of the facts, the obtained hydrodynamic diameters D_{DLS} are very close to the diameters from SEM microscopy (see in Table 1).

The same equipment was applied to measure zeta potential to give us information about the value of surface charge the studied nanoparticles. All coated MNPs were negatively charged, zeta potentials were determined to be −42, −37, −42, and −50 mV for the samples MF, MFBSA, MFPEG, and PLGA-MFPEG, respectively (see Table 1). As value of zeta potential is directly proportional to stability of nanoparticles, (e.g. higher absolute value of zeta potential means that nanoparticles colloidal system will be more stable), we could summarize that the samples are colloidal stable. Although positively charged nanoparticles have been shown to improve the efficacy of imaging, and drug delivery due to electrostatic attraction to the negatively charged cell membrane, they are more toxic and produce superior local immune responses than negatively charged ones [23].

The quantification of modifying compound amount on MNPs was conducted by TGA. The theoretical loading weight ratio of modifying agent to MNPs was as follows BSA/Fe_3O_4 = 2, PEG/Fe_3O_4 = 0.25 and PLGA/Fe_3O_4 = 2. The determined weight losses of organic coatings at T = 650 °C, temperature at which the samples decomposed almost completely, are summarized in Table 1. The amount of organic coating per magnetite amount was then derived by taking the residue of organic mass (wt%) and dividing by the resulting magnetite weight after water loss determined before coating.

The magnetic properties were evaluated for all samples in liquid suspensions by magnetic measurements at room temperature (Fig. 2). The saturation magnetization values of MFBSA (2.74 emu/g), MFPEG (2.06 emu/g) and PLGA-MFPEG (1.87 emu/g) covered with BSA, PEG, or PLGA, respectively, are slightly lower than those of the starting MF (2.66 emu/g). This decrease in saturation magnetization is due to the increase in total mass, e.g. the presence of a non-magnetic phase (coating) in the sample. The saturation magnetizations (*Ms*) of individual MNPs are presented in Table 1. Moreover, the absence of both remanent magnetization and coercivity field confirm superparamagnetic behaviour in all the prepared samples in this study. To extract information about the magnetic core diameter (D_{LF}) of particular MNPs, the experimental magnetization was fitted by Langevin function. Obtained size distributions are shown as insets in Fig. 2 and diameters are summarized in Table 1 as well.

Once entering the biological fluids, the surface of nanoparticles is rapidly covered by proteins to form a corona ('soft' and 'hard' protein corona). For majority of NPs, the corona is dominated by albumin, the most abundant protein in serum (55%); however, lower abundance proteins, such as immunoglobulins, apolipoproteins, and fibrinogen, are also found in the corona [24]. The corona composition depends on the physicochemical properties (e.g. surface chemistry, size, shape, charge etc.) of the particle, which in turn determines the interactions between NP and cells/tissue and also might predict any adverse cellular responses [25]. The colloidal stability and particle size distribution of nanoparticles in culture medium (DMEM + 2% FCS + 1% ATB) was performed by DLS, and the data are presented in Table 2. A substantial increase in the hydrodynamic particle size due to adhesion of serum proteins to the particle surface has been determined in all surface-modified MNPs. The greatest change in particle size was observed in PLGA-MFPEG while the smallest increase in particle size was determined in MFBSA. Additionally, MF, MFBSA and MFPEG dispersions in culture medium were stable at least for 24 h while PLGA-MFPEG particles were less stable, and were prone to precipitate slowly after 24 h. The zeta potential of all surface modified MNPs increased to less negative values in culture medium compared to stock MNPs dispersions in deionized water; the values of zeta potential ranged from −18.8 to −16.3 mV.

3.2. Heat generation of nanoparticles in AMF

The ability of some magnetic nanoparticles to transform magnetic energy into heat has recently emerged as a prospective therapeutic option in the treatment of cancer [26]. A part of the energy absorbed by a sample under an AMF undergoes irreversible conversion into thermal energy and results as heat. For superparamagnetic nanoparticles the physical principle of heating is due to Néel and Brownian relaxation processes [27,28]. The capacity of surface coated MNPs to generate heat was measured at various magnetic field intensities and constant frequency 252 kHz in AMF. From the monitored time evolution of temperature, the dT/dt was estimated as a linear fit of the temperature *vs.* time dependences for all samples at each of the applied AMF intensity. Obtained heating rates dT/dt were subsequently plotted as a function of the AMF intensity (Fig. 3A). With increasing AMF the dynamics of the temperature increase, slope ($\sim dT/dt$) became much steeper as well. The experimental points were fitted by the function $(H/a)^n$. where the a and n are fitting parameters which depend on many particle features, such as permeability, conductivity, shape, and size distribution. Exponent "n" for all dT/dt *vs* H dependencies was approx. 2, so temperature increased with increasing field intensity H^2. It agrees with Rosensweig's claim [29] that for magnetic fluid with particle mean size of 10 nm in AMF the power dissipation increases with H^2. The time dependent temperature changes for tested magnetic fluid samples were used to determine the specific absorption rate (SAR) values. The SAR is defined as the amount of heat released by a unit weight of the material per unit of time during exposure to an oscillating magnetic field of a given frequency and field strength [30] (Eq. (5))

$$SAR = \frac{C_p \rho_s}{m}\left(\frac{dT}{dt}\right)[Wg^{-1}] \quad (5)$$

where Cp (4.18 J/K·g) and ρ_s (kg/m^3) are the specific heat and density of the sample, respectively, and m is the mass of magnetite per unit volume of the colloid.

The SAR values obtained at AMF frequency f = 252 kHz and maximum applied field intensity H = 23.9 kA/m are shown in Fig. 3B. The SAR values at this condition reached approx. 13–16 W/g, e. g. values show no significant difference, therefore we can conclude that coating shell do not have influence on SAR what is in accordance with results presented in paper [31].

3.3. Biological effects of MNPs

Representative images of A549 cells treated with surface modified MNPs at 0, 12, 18 and 24 h are shown in Fig. 4. For this analysis, subtoxic concentrations (viability > 70%) was selected. Some changes in cell morphology were observed in all MNP-exposed cells already after 12 h of treatment. The MNPs-treated cells acquired more fibroblastoid shapes, and became grainy. The most visible changes were observed in MF- and MFPEG-treated cells while the impact of MFBSA and PLGA-MFPEG particles on A549 cell morphology was less apparent.

All types of MNPs induced a dose-dependent decrease in cell viability after 24 h treatment (Fig. 5A). The cytotoxicity of particular MNPs correlated with the hydrodynamic size of MNPs (Table 1). Moreover, differences in cell toxicity were determined in dependence on the surface coating. The strongest inhibition of cell growth was determined in PLGA-MFPEG treated A549 cells, while MF particles

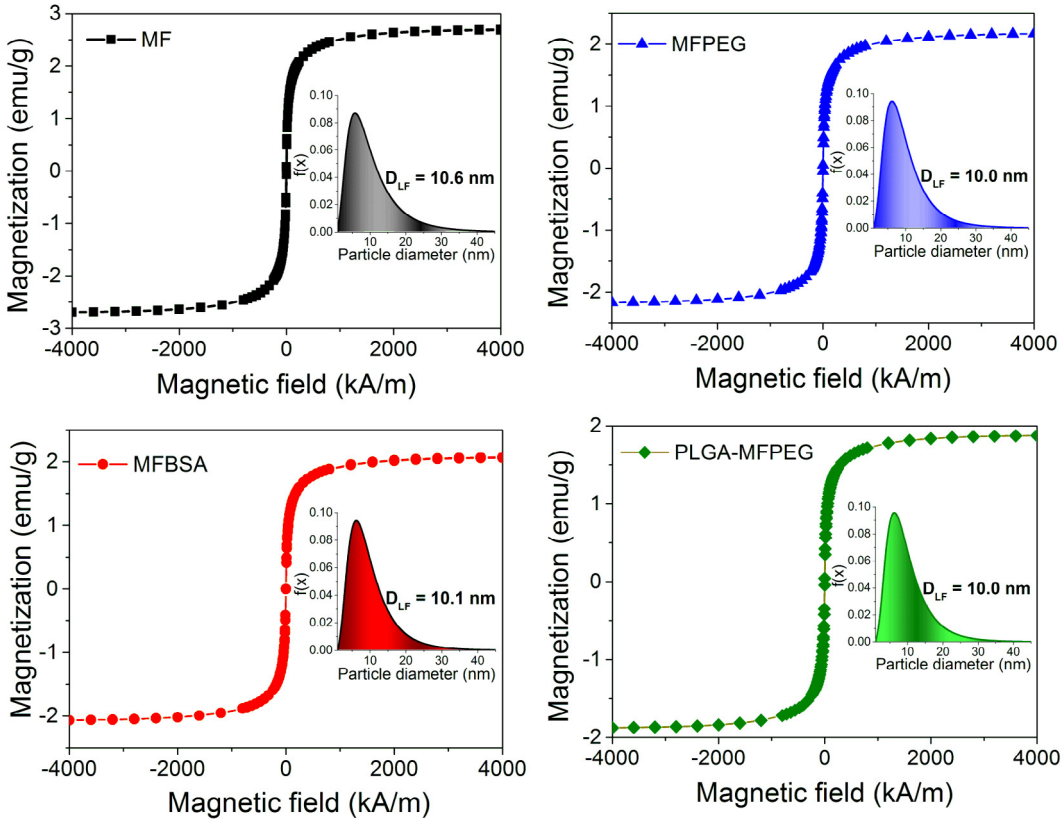

Fig. 2. Magnetization curves of MF, MFBSA, MFPEG, and PLGA-MFPEG measured at room temperature. Size distribution of the magnetic cores obtained by fitting magnetization curves by Langevin function (insets).

were less cytotoxic. As PLGA is a US-FDA approved polymer for clinical applications, the strong toxicity is probably not primarily caused by the coating. The large hydrodynamic size of PLGA-MFPEG in culture medium (> 555 nm) underlies colloidal instability of this dispersion resulting in slow sedimentation the bottom of the plate. We can speculate that these MNPs might form a thin layer over the adherent cells. This thin film might in turn disturb the normal cellular physiological functions due to mechanical stress, disruption of nutrition intake and intercellular communication. It has been shown that mechanical stress [32], nutrient starvation, oxidative and energetic stresses [33] can induce autophagy in most cell types.

In general, oxidative stress and generation of reactive oxygen species (ROS) are supposed to underlie the toxicity of nanoparticles, particularly iron oxide nanoparticles. Based on our previous results, oxidative stress plays, at most, only a marginal role in the genotoxicity of these surface modified MNPs in lung cells [17]. On the other hand, we have shown that these surface modified MNPs are able to interfere with tubulin polymerization leading to disrubtion of cytoskeletal structure and chromosome malsegregation [34]. Cytoskeleton plays an important role in many cellular physiological functions such as cell division, cell morphology, cell signaling and cell motility. Functional constraints due to disturbance of cytoskeleton network might underlie the changes in cell morphology and viability.

Substantial differences in the internalized amount of surface modified MNPs were determined in A549 cells (Fig. 5B). MFBSA and PLGA-MFPEG were taken up less efficiently (0.39 and 0.70 pg/cell, respectively) in comparison with MFPEG and MF (2.58 and 1.93 pg/cell, respectively). The particle size has been shown to determine the mechanism of the uptake. Larger nanoparticles (100–150 nm) are supposed to be taken up *via* clathrin-mediated endocytosis (CME), while smaller particles (50–80 nm) are internalised by caveolin-mediated endocytosis (CavME). However, the data published so far lack concordance about the threshold diameter determining the particular pathway of endocytosis the nanoparticles are taken up. There is growing evidence that the composition of protein corona can strongly affect cellular internalization of nanoparticle [35]. Using the specific inhibitors of endocytosis, we have found that MFBSA are internalized by CME pathway while MFPEG are taken up by CavME (manuscript under preparation). In line with our results, Lewinski et al. [36] and Kim et al. [37] have shown that MNPs with the hydrodynamic size around 80 nm are internalized by CME. Our preliminary results indicate that MF and PLGA-MFPEG particles might be internalized by CavME, however, the role of macropinocytosis or CME and CavME pathways cannot be excluded. MNP uptake is a complex process influenced by the characteristics of MNPs (size, shape, coating, stability, solubility, surface charge, etc.) and their availability for cell on one hand, and by the

Table 2
Characteristics of colloidal dispersions of surface modified MNPs in culture medium.

MNPs	C (Fe_3O_4) [mM]/[μg/mL]	D_{DLS} [nm]	*PDI*	Zeta potential [mV]	Stability [24 h]
MF	0.3/69.45	244 ± 6	0.173 ± 0.017	−14.6 ± 0.9	stable
MFBSA	0.3/69.45	98 ± 8	0.138 ± 0.012	−16.3 ± 0.9	stable
MFPEG	0.3/69.45	281 ± 4	0.169 ± 0.011	−13.8 ± 0.9	stable
PLGA-MFPEG	0.3/69.45	555 ± 161	0.386 ± 0.045	−14.7 ± 1.2	unstable

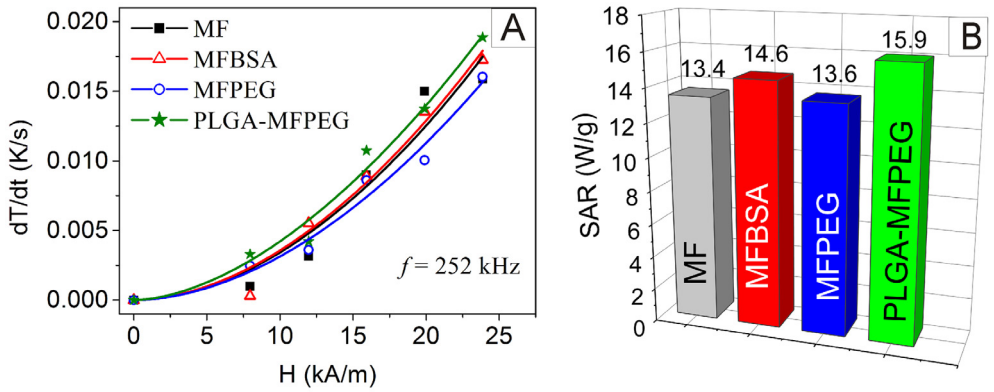

Fig. 3. Dependence of dT/dt on the AMF intensity H at a frequency $f = 252$ kHz for each MNP sample (A). SAR values of MF, MFBSA, MFPEG and PLGA-MFPEG in the applied AMF ($f = 252$ kHz, $H = 23.9$ kA/m) (B).

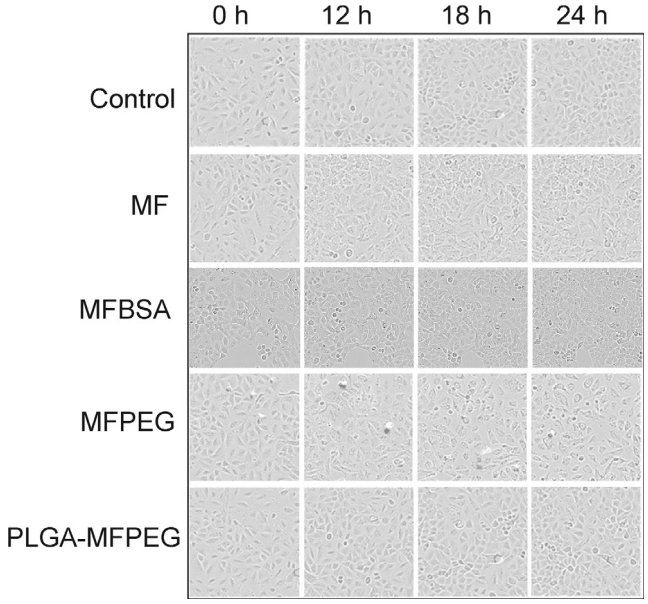

Fig. 4. The impact of surface modified magnetic iron oxide nanoparticles on cell morphology. A549 cells were treated with MF (0.5 mM), MFBSA (0.5 mM), MFPEG (0.3 mM), PLGA-MFPEG (0.15 mM) for 24 h. Phase-contrast images of treated cells at 0 h, 12 h, 18 h and 24 h (magnification 40x).

biological factors (mechanism of endocytosis, cell type, cell density, cell fitness, etc.) on the other hand [34,38]. Further experiments are required to determine the mechanism(s) of uptake of particular surface modified MNPs.

4. Conclusion

MNPs with magnetite inner core diameter of ~10 nm and hydrophilic outer shell of surfactant, protein and polymers that are widely used in biomedical research were prepared. Coated MNPs were spherical in shape with mean hydrodynamic diameter in range of 40–155 nm in dependence of used modifying agent. All magnetic fluids exhibit superparamagnetic behaviour at room temperature. The heating characteristics of the magnetic fluid samples (unmodified as well as modified) were studied by magnetic hyperthermia and no influence of modified layer thickness on SAR was found. However, the coating material and the resulting surface charges are of high importance for cellular uptake, and biocompatibility. Cytotoxicity study showed that A549 cells exposed to surface modified MNPs for 24 h caused a dose-dependent decrease in cell proliferation. MF with the smallest hydrodynamic size (44 nm) were at least two-fold less cytotoxic than the larger MFPEG and PLGA MFPEG (D_{HYDR} = 76 nm and 155 nm, respectively). MFPEG and MF were taken up by A549 cells more efficiently that MFBSA and PLGA-MFPEG. Further experiments are required to specify the mechanism of MNPs internalization.

Acknowledgements

This work was supported by Slovak Research and Development Agency under the contracts Nos. APVV-14-0120, APVV-14-0932, and APVV-15-0453, the Scientific Grant Agency contracts Nos. 2/0056/17, 2/0113/15, 2/0016/17 and 2/0141/16, by project co-financed from EU sources PROMATECH (ITMS No. 26220220186), Center of

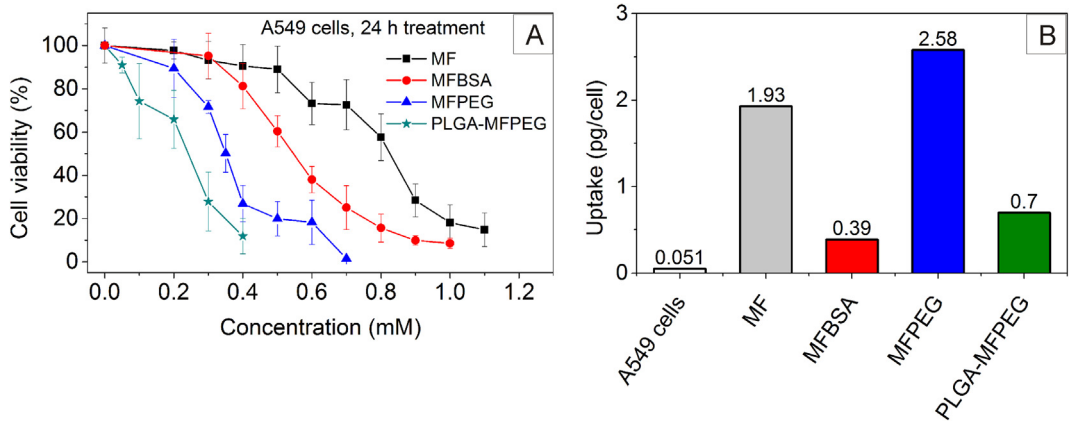

Fig. 5. Cytotoxicity of MF, MFBSA, MFPEG, and PLGA-MFPEG in A549 cells after 24 h treatment (A), and the internalized amount of surface modified MNPs (B).

excellence of environmental health (ITMS No. 26240120033), and by the H2020 (H2020/2014-2020) funding under Grant agreement 685817 – HISENTS and by the grant EEA FM and the NFM (Project SK0020). The authors thank to the European COST action TD1402 (RADIOMAG) and to MagBioVin: supported by the European Commission through the Project MagBioVin, grant agreement no: 621375. The authors would like to acknowledge Drs. F. Razga and V. Nemethova for assessment the colloid stability of surface modified MNPs in culture medium.

Appendix A. Supplementary data

Supplementary data to this article can be found online at https://doi.org/10.1016/j.jmmm.2018.09.116.

References

[1] Q. Mu, G. Jiang, L. Chen, H. Zhou, D. Fourches, A. Tropsha, B. Yan, Chemical basis of interactions between engineered nanoparticles and biological systems, Chem. Rev. 114 (2014) 7740–7781, https://doi.org/10.1021/cr400295a.
[2] A. Albanese, P.S. Tang, W.C. Chan, The effect of nanoparticle size, shape, and surface chemistry on biological systems, Annu. Rev. Biomed. Eng. 14 (2012) 1–16, https://doi.org/10.1146/annurev-bioeng-071811-150124.
[3] E. Susan, Apoptosis: a review of programmed cell death, Toxicol. Pathol. 35 (2007) 495–516, https://doi.org/10.1080/01926230701320337.
[4] H. Zhang, N. Huang, G. Yang, Q. Lin, Y. Su, Bufalin-loaded bovine serum albumin nanoparticles demonstrated improved anti-tumor activity against hepatocellular carcinoma: preparation, characterization, pharmacokinetics and tissue distribution, Oncotarget 8 (2017) 63311–63323, https://doi.org/10.18632/oncotarget.18800.
[5] C.T. Sengel-Turk, C. Hascicek, A.L. Dogan, G. Esendagli, D. Guc, N. Gonul, Surface modification and evaluation of PLGA nanoparticles: the effects on cellular uptake and cell proliferation on the HT-29 cell line, J. Drug Del. Sci. Technol. 24 (2014) 166–172, https://doi.org/10.1016/S1773-2247(14)50027-5.
[6] I. Antal, M. Kubovcikova, V. Zavisova, M. Koneracka, O. Pechanova, A. Barta, M. Cebova, V. Antal, P. Diko, M. Zduriencikova, M. Pudlak, P. Kopcansky, Magnetic poly(d, l-lactide) nanoparticles loaded with aliskiren: a promising tool for hypertension treatment, J. Magn. Magn. Mater. 380 (2015) 280–284, https://doi.org/10.1016/j.jmmm.2014.10.089.
[7] M.C. Hacker, A.G. Mikos, Synthetic Polymers in Principles of Regenerative Medicine (second ed.), 2011, pp. 587–622, doi: 10.1016/B978-0-12-381422-7.10033-1.
[8] A.H. Faraji, P. Wipf, Nanoparticles in cellular drug delivery, Bioorg. Med. Chem. 17 (2009) 2950–2962, https://doi.org/10.1016/j.bmc.2009.02.043.
[9] I. Khan, A. Gothwal, A.K. Sharma, P. Kesharwani, L. Gupta, A.K. Iyer, U. Gupta, PLGA nanoparticles and their versatile role in anticancer drug delivery, Crit. Rev. Ther. Drug Carrier Syst. 33 (2016), https://doi.org/10.1615/CritRevTherDrugCarrierSyst. 2016015273.
[10] I. Khmara, M. Koneracka, M. Kubovcikova, V. Zavisova, I. Antal, K. Csach, P. Kopcansky, I. Vidlickova, L. Csaderova, S. Pastorekova, M. Zatovicova, Preparation of poly-L-lysine functionalized magnetic nanoparticles and their influence on viability of cancer cell, J. Magn. Magn. Mater. 427 (2017) 114–121, https://doi.org/10.1016/j.jmmm.2016.11.014.
[11] M. Kubovčíková, I. Antal, J. Kováč, V. Závišová, M. Koneracká, P. Kopčanský, Preparation and complex characterization of magnetic nanoparticles in magnetic fluid, Acta Phys. Pol. A 126 (2014) 268–269, https://doi.org/10.12693/APhysPolA.126.268.
[12] V. Zavisova, M. Koneracka, J. Kovac, M. Kubovcikova, I. Antal, P. Kopcansky, M. Bednarikova, M. Muckova, The cytotoxicity of iron oxide nanoparticles with different modifications evaluated in vitro, J. Magn. Magn. Mater. 380 (2015) 85–89, https://doi.org/10.1016/j.jmmm.2014.10.041.
[13] V. Zavisova, M. Koneracka, M. Muckova, J. Lazova, A. Jurikova, G. Lancz, N. Tomasovicova, M. Timko, J. Kovac, I. Vavra, M. Fabian, A.V. Feoktystov, V.M. Garamus, M.V. Avdeev, P. Kopcansky, Magnetic fluid poly(ethylene glycol) with moderate anticancer activity, J. Magn. Magn. Mater. 323 (2011) 1408–1412, https://doi.org/10.1016/j.jmmm.2010.11.060.
[14] N. Tomasovicova, I. Khmara, M. Koneracka, V. Zavisova, M. Kubovcikova, I. Antal, J. Kovac, M. Muckova, P. Kopcansky, Elimination of magnetic nanoparticles with various surface modifications from the bloodstream in vivo, Acta Phys. Pol. A 4 (2017) 1159–1161, https://doi.org/10.12693/APhysPolA.131.1159.
[15] M. Kubovčíkova, I. Antal, M. Koneracká, V. Závišová, K. Šípošová, Z. Gažová, J. Kováč, M. Kovarik, D. Kupka, P. Kopčanský, Magnetic nanoparticles modified with polyethylene glycol, Magnetohydrodynamics 49 (2013) 282–286.
[16] H. Fessi, F. Puisieux, J.Ph. Devissaguet, N. Ammoury, S. Benita, Nanocapsules formation by interfacial deposition following solvent displacement, Int. J. Pharm. 55 (1989) R1–R4, https://doi.org/10.1016/0378-5173(89)90281-0.
[17] M. Mesárošová, K. Kozics, A. Bábelová, E. Regendová, M. Pastorek, D. Vnuková, B. Buliaková, F. Rázga, A. Gábelová, The role of reactive oxygen species in the genotoxicity of surface-modified magnetite nanoparticles, Toxicol Lett. 226 (2014) 303–313, https://doi.org/10.1016/j.toxlet.2014.02.025.
[18] R.W. Chantrell, J. Popplewell, S.W. Charles, Measurements of particle-size distribution parameters in ferrofluids, IEEE Trans. Magn. 14 (1978) 975–977, https://doi.org/10.1109/TMAG.1978.1059918.
[19] Z. Rozynek, A. Jozefczak, K.D. Knudsen, A. Skumiel, T. Hornowski, J.O. Fossum, M. Timko, P. Kopcansky, M. Koneracka, Structuring from nanoparticles in oil-based ferrofluids, Eur. Phys. J. E 34 (2011) 1–8, https://doi.org/10.1140/epje/i2011-11028-5.
[20] T. Mosmann, Rapid colorimetric assay for cellular growth and survival: application to proliferation and cytotoxicity assays, J. Immunol. Methods 65 (1983) 55–63, https://doi.org/10.1016/0022-1759(83)90303-4.
[21] U.O. Hafeli, J.S. Riffle, L. Harris-Shekhawat, A. Carmichael-Baranauskas, F. Mark, J.P. Dailey, D. Bardenstein, Cell uptake and in vitro toxicity of magnetic nanoparticles suitable for drug delivery, Mol. Pharm. 6 (2009) 1417–1428, https://doi.org/10.1021/mp900083m.
[22] M. Koneracka, M. Múčková, V. Závišová, N. Tomašovičová, P. Kopčanský, M. Timko, A. Juríková, K. Csach, V. Kavečanský, G. Lancz, Encapsulation of anticancer drug and magnetic particles in biodegradable polymer nanospheres, J. Phys.: Condens. Matter. 20 (2008), https://doi.org/10.1088/0953-984/20/20/204151 204151 (6pp).
[23] E. Fröhlich, The role of surface charge in cellular uptake and cytotoxicity of medical nanoparticles, Int. J. Nanomed. 7 (2012) 5577–5591, https://doi.org/10.2147/IJN.S36111.
[24] C.C. Fleischer, C.K. Payne, Nanoparticle-cell interactions: molecular structure of the protein corona and cellular outcomes, Acc. Chem. Res. 47 (8) (2014) 2651–2659, https://doi.org/10.1021/ar500190q.
[25] M. Mahmoudi, N. Bertrand, H. Zope, O.C. Farokhzad, Emerging understanding of the protein corona at the nano-bio interfaces, Nano Today 11 (2016) 817–832, https://doi.org/10.1016/j.nantod.2016.10.005.
[26] M. Bañobre-López, A. Teijeiro, J. Rivas, Magnetic nanoparticle-based hyperthermia for cancer treatment, Rep. Practical Oncol. Radiother. 18 (2013) 397–400, https://doi.org/10.1016/j.rpor.2013.09.011.
[27] D. Ortega, Q.A. Pankhurst, Magnetic hyperthermia, Nanoscience 1 (2012) 60–88, https://doi.org/10.1039/9781849734844-00060.
[28] M. Molcan, H. Gojzewski, A. Skumiel, S. Dutz, J. Kovac, M. Kubovcikova, P. Kopcansky, L. Vekas, M. Timko, Energy losses in mechanically modified bacterial magnetosomes, J. Phys. D. Appl. Phys. 49 (2016), https://doi.org/10.1088/0022-3727/49/36/365002.
[29] R.E. Rosensweig, Heating magnetic fluid with alternating magnetic field, J. Magn. Magn. Mater. 252 (2002) 370–374, https://doi.org/10.1016/S0304-8853(02)00706-0.
[30] A. Skumiel, M. Kaczmarek-Klinowska, M. Timko, M. Molcan, M. Rajnak, Evaluation of power heat losses in multidomain iron particles under the influence of AC magnetic field in RF range, Int. J. Thermophys 34 (2013) 655–666, https://doi.org/10.1007/s10765-012-1380-0.
[31] R. Ludwig, M. Stapf, S. Dutz, R. Müller, U. Teichgräber, I. Hilger, Structural properties of magnetic nanoparticles determine their heating behavior – an estimation of the in vivo heating potential, Nanoscale Res. Lett. 9 (2014) 602, https://doi.org/10.1186/1556-276X-9-602.
[32] J.S. King, D.M. Veltman, R.H. Insall, The induction of autophagy by mechanical stress, Autophagy 7 (12) (2011) 1490–1499, https://doi.org/10.4161/auto.7.12.17924.
[33] Y.-Y. Chang, G. Juhász, P. Goraksha-Hicks, A.M. Arsham, D.R. Mallin, L.K. Muller, T.P. Neufeld, Nutrient-dependent regulation of autophagy through the target of rapamycin pathway: Figure 1, Biochem. Soc. Trans. 37 (2009) 232–236, https://doi.org/10.1042/BST0370232.
[34] B. Buliaková, M. Mesárošová, A. Bábelová, M. Šelc, V. Némethová, L. Šebová, F. Rázga, M. Ursínyová, I. Chalupa, A. Gábelová, Surface-modified magnetite nanoparticles act as aneugen-like 2 spindle poison, Nanomedicine 13 (2017) 69–80, https://doi.org/10.1016/j.nano.2016.08.027.
[35] V. Mirshafiee, V. Mirshafiee, R. Kim, S. Park, M. Mahmoudi, M.L. Kraft, Impact of protein pre-coating on the protein corona composition and nanoparticle cellular uptake, Biomaterials 75 (2016) 295–304, https://doi.org/10.1016/j.biomaterials.2015.10.019.
[36] N. Lewinski, V. Colvin, R. Drezek, Cytotoxicity of nanoparticles, Small 4 (2008) 26–49, https://doi.org/10.1002/smll.200700595.
[37] J.S. Kim, T.J. Yoon, K.N. Yu, M.S. Noh, M. Woo, B.G. Kim, K.H. Lee, B.H. Sohn, S.B. Park, J.K. Lee, M.H. Cho, Cellular uptake of magnetic nanoparticle is mediated through energy-dependent endocytosis in A549 cells, J. Vet. Sci. 7 (2006) 321–326, https://doi.org/10.4142/jvs.2006.7.4.321.
[38] V. Némethová, B. Buliaková, P. Mazancová, A. Bábelová, M. Šelc, D. Moravčíková, L. Kleščíková, M. Ursínyová, A. Gábelová, F. Rázga, Intracellular uptake of magnetite nanoparticles: a focus on physico-chemical characterization and interpretation of in vitro data, Mater. Sci. Eng., C 70 (2017) 161–168, https://doi.org/10.1016/j.msec.2016.08.064.